Contents lists available atGrowingScience

Engineering Solid Mechanics

homepage: www.GrowingScience.com/esm

Optimization of non-bearing splice connection in GFRP short columns by manual testing and finite element analysis

M. J. Srujan[a] and Seelam Srikanth[a*]

[a]*REVA University, India*

ARTICLEINFO

Article history:
Received 23 May 2023
Accepted 11 January 2024
Available online
11 January 2024

Keywords:
GFRP
FEA
Spliced connection
Axial load

ABSTRACT

Connection designs are established to ensure the stability of joined cut sections, the joints so designed should be based on the optimal performance as per the requirements. The connection joints so established should not be based on just strength but reliability and durability as well. This study focuses on tackling one of the major issues faced when using Glass Fibre Reinforced Polymers (GFRPs) as construction materials, which is based on the abrupt failure of the material under critical or maximum loading. Connection designs are established in GFRP short column H-sections based on Bolted Splicing connections by Eurocode 3 for steel splicing connections. A total of seven Connection designs are established using bearing and non-bearing splicing connections. A total of five models for each connection is established for manual testing and Finite Element Analysis (FEA) is used to simulate and analyze these connection designs. Parameters such as ultimate load, displacement at ultimate load, stiffness, compressive strength, failure mode, load versus displacement behavior graph, and percentage compressive strength compared to the un-cut section are provided in this study. The strongest specimen in this study displaced 128% and 127.7% compressive strength compared to an un-cut GFRP H-section when tested using manual testing and FEA accordingly.

1. Introduction

Fibre Reinforced Polymers (FRPs) are composite materials that contain dense layers of fibres embedded in an adhesive matrix (Sorrentino et al., 2017). These FRPs provide high strength at a low weight which makes them a popular choice of material in the aerospace industry since the mid-20th century (Anand & Patra, 2017). Glass Fibre Reinforced Polymer (GFRP) is a type of FRP that is made of multiple thin layers of glass fibres in a complex mesh design, they are compressed under high pressure with a resign to derive a solid structure (Liu et al., 2018). These GFRPs can be molded into various shapes and sizes depending on the requirement and do not require heat application for achieving any structural alterations which reduces the carbon footprint of the material in the manufacturing process (Yoon et al., 2020). GFRPs possess high structural strength but are brittle in nature as they fail abruptly at maximum loading. The brittle nature also restricts the structure from being malleable and ductile. But, they possess numerous advantages such as electrical insulation, fire resistance, high thermal capacity, non-corrosive, low toxic emission, dynamic loading resistance, and high strength-to-weight ratio (Li et al., 2017). In contrast with their advantages and disadvantages, GFRPs are considered good composite materials which are used for retrofitting and to produce light weight parts in the automobile and aerospace industry (Cepero-Mejías et al., 2020).

GFRPs due to their materialistic properties are becoming popular in the construction industry (Esmaeili et al., 2018). The use of these materials significantly decreases the dead loads of the structure making structural members smaller and more static (Hocheng and Tsao, 2005). Long-span structures with significantly lower dead loads compared to traditional RCC structures can be achieved by using GFRPs as composite construction materials (Rahmé et al., 2011). Coastal structures when

* Corresponding author.
E-mail addresses: srikanths.reddy@reva.edu.in (S. Srikanth)

ISSN 2291-8752 (Online) - ISSN 2291-8744 (Print)

doi: 10.5267/j.esm.2024.1.005

built with steel tend to hold various disadvantages with corrosion being a major driver in the deterioration of the structural integrity (Sadowski et al., 2019). The non-corrosive characteristics of the material with high thermal capacity and fire resistance are some of the characteristics that is making GFRP popular as a construction material for marine-based projects (Phadnis et al., 2013). In industries that require heavily engineered structures such as the petrochemical and shipping industry GFRPs are proven to be highly advantageous over previously used traditional material (Suemasu et al., 2012). The workability of GFRP is similar to that of steel except for the convenience of welding that steel offers (Camanho and Catalanotti, 2018). That is, steel structures can be connected by welding, bolting, and riveting. Similarly, GFRP structures can be bolted, bonded, and riveted but cannot be welded (Geng et al., 2019). Bonding of structures is a complicated procedure and requires higher skilled labor compared to welding (Voß et al., 2016). This is a major drawback of using the material in the construction industry (Girot et al., 2017). High-strength bonding substances or adhesives can be used to establish such a connection, but the bond environment and restrictions play a vital role in achieving the desired strength of the bond (Stone and Krishnamurthy, 1996; Paroissien et al., 2017). Rapid curing adhesives with high peel-off strength or rupture strength are recommended for bonded GFRP structures to reduce professional labor-intensive work on the construction site (Curiel-Sosa et al., 2018).

Bonds also play a major role in establishing the homogenous nature of the material for GFRP structures as welding does for steel structures (Zhang et al., 2021). The high strength with low displacement at failure is advantageous in industries that require the material not to disintegrate into fragments at failure (Wang et al., 2018). But, for structural construction, the low displacement at maximum loading can be fatal at the time of structural failure or collapse (Bodjona et al., 2015). To maintain the safety of the habitats of a structure, the building is expected to display signs of failure to provide a safety signal or time to evacuate the place (Al-wandi et al., 2017). If the structure is to fail abruptly, the damages can be catastrophic (Baha, 2015). This is a major disadvantage of using the material for constructing structures, especially in regions where variable loading can be expected (Turki et al., 2014). The load vs displacement graph of steel comprises an elastic region and a plastic region and failure happens with a significantly larger displacement value (Kwon et al., 2019). Whereas for GFRPs the load vs displacement graph displays a sudden drop in the load-bearing capacity of the material with very little displacement and no yield point before the point of failure at ultimate loading (Feito et al., 2018; Gamdani et al., 2019). This characteristic can be tackled using the concept of robustness when using GFRP as a building material. Robustness in structural design is an aspect of the structure that requires it to be strong and to satisfy the ideal safety conditions (Samaei et al., 2016). GFRP as a building material is strong but for the material to be used for construction it has to be strong and safe. Hence, the concept of robustness should be introduced in the design of GFRP structures as safety is an important criterion of structural design and development (Zou et al., 2017).

To establish a stable or robust connection in framed structures two aspects of design should be satisfied, namely the connection technique or connection methods, and the type of connection (Shahkhosravi et al., 2019; Carbas et al., 2020). The connection techniques used in GFRP framed structures are bonded, bolted, and hybrid connection methods (Chowdhury et al., 2016). Whereas there are various types of connection methods used in GFRP framed connection structures the commonly used ones being seated plate connection, end plate connection, pinned connection, moment connection or rigid connection, spliced connection, and shear connection or flexible connection (Zuo et al., 2020; Liu et al., 2014). Robustness as a structural design concept can be introduced by adding a degree of cut-off or structural fuse in the design of the connection (Liu et al., 2013; Chen et al., 2019). The trigger or the fuse is used as a sign of warning regarding the possibility of structural failure, or it can also be used for deriving a time bracket before the structure fails (Banea et al., 2018). Globally most of the standard structural codes such as the International Building Code, Canadian Standards Association, Australian Standards, and Indian Standards Code do not encourage the concept of a structural fuse (Ascione et al., 2010). But they enhance the structure by increasing the Factor of Safety (FOS) of the structure. Having a higher FOS makes the structure bulky and does not satisfy the robustness criteria of GFRP structures (Yuanxin et al., 2015; Zhang et al., 2019). Due to the absence of design codes for GFRP structural design in all standard codes, steel structure connection techniques can be implemented for designing connections of any rigid or semi-rigid building material (Heidary et al., 2018). The borrowing of design from a standard structural design code for a material that is considered as a replacement of the ideal material mentioned in the codes helps in satisfying and validating principal conditions of material replacement and structural requirements (Krishnaraj et al., 2012; Marques et al., 2016). GFRP as a structural material is considered a replacement for traditional steel as a building material so designing a GFRP structure following steel structural design provides material replacement details and helps assess the behavioral characteristics of the two materials.

Euro code, unlike other standard structural design codes, provides provisions for structural fuse and framed structures, Euro Code 3 holds a connection called non-bearing spliced connection, which is a connection technique that connects two frames using cover plates, bolts, and a splicing gap (Makhdum et al., 2014). Splicing is a connection method that reinforces the joint using packing material called cover plates by utilizing connection techniques such as bolting and riveting (Heidary and Mehrpouya, 2019). Non-bearing Splicing connection is an advanced splicing method that involves a provision of a gap called the splicing gap which is provided between the two-connection structure to act as a fuse (Lü et al., 2016). As the gap closes the displacement of the overall structure increases thereby displaying failure characteristics and post-failure due to the material property of the structural element a fraction of extra strength can be derived by using such connections (Bodjona et al., 2015; Selahi, 2019). Euro code 3 provides the splicing regulations with all the provisions for allowable splicing gap, cover plate positioning, bolting specifications, and tightening conditions for the bolts (Bois et al., 2013). This design specification

when implemented on GFRP structures will induce the robustness characteristic hence meeting the design criteria and safety standards for using the material as a construction material (Goldarag et al., 2015).

The experimental investigation of slicing connection which variation in the splicing gap along with the length of the short column on the joint behavior is examined in this research (Raju et al., 2016). Bearing a splicing connection without a splicing gap is examined to determine the strength of the connection without a splicing gap and to derive an idea of the failure behavior. An uncut GFRP short column is also crushed to identify the compressive strength of the material and to derive the relative strength of the connected GFRP structure when compared to an un-cut GFRP structure. The mode of testing is carried out using FEA and manual testing to have verifying results and to derive ideal connection conditions (Shetty et al., 2017).

2. Experimental program

Two phases of design and testing are involved in the optimization of the robust spliced GFRP H-section short-column connection. Phase-1 involves the designing and testing of the Splicing Gap specifications for the joint. Phase-2 involves the height of the short column and the short column conditions for GFRP H-sections. Based on the results from Phase-1, the Phase-2 models are designed. All the models are tested Manually and using FEA to obtain optimal comparable results.

Phase-1 involves the design and creation of four modes with five samples in each model. The design is based on the length of the splicing gap that is provided in the joint as shown in **Fig. 1**. The first set of samples from the model M-G0-H350 hold no splicing gap, which makes these samples a Bearing splicing connection. This model is created as an example to display the strength of the splicing connection by using cover plates as joint reinforcements. The samples from model M-G15-H350 hold a splicing gap of 15mm in them based on the minimum regulations from the Eurocode 3 regulations. This connection is a non-bearing splicing connection. The gap of 15mm is selected as the minimum slicing gap over other standard values to satisfy the late offset of the structural fuse condition. An early offset of a structural fuse by using splicing gaps of about 10mm or 5mm will not hold practicality if a pseudo failure triggers the splicing gap to close. The samples from M-G25-H350 are selected based on the standards as mentioned in Eurocode 3 for the design of non-bearing Spliced connections. These samples are specified as per the working guidelines from Eurocode 3 for Non-bearing Spliced Steel H-section connection from BS EN 1990 and BS EN 1991. The samples from model M-G30-H350 hold a splicing gap of 30mm in them. The increase of a 5mm gap from the standards as mentioned in Eurocode 3 is done in these models to verify the reason behind holding a standard splicing gap value in the code.

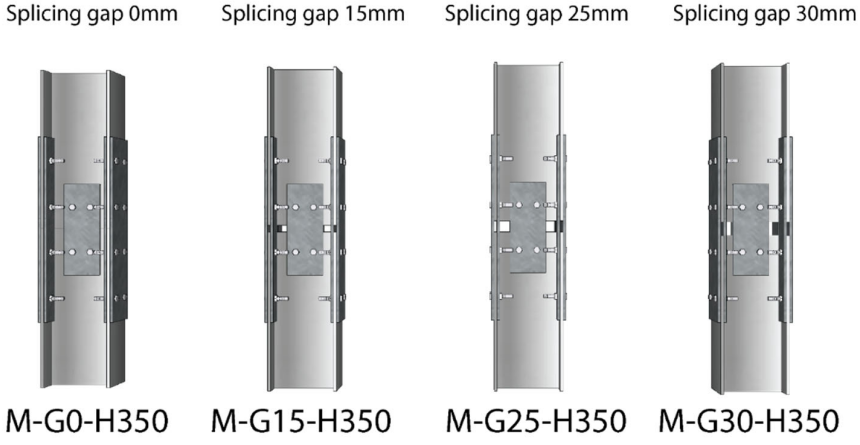

Fig. 1. Designs for model specimens of phase-1

After testing the models from Phase-1 the models from Phase 2 are created. The models are created based on the short column condition for testing GFRP H-sections as shown in **Fig. 2.** A total of 5 samples are created for each model to generate accurate joint behavior of the connection. The samples from model M-G25-H300 are designed based on the shortest column that can be tested based on there being adequate space from the joint to the region of load application. There is a clearance of 100mm from the joint to the top of the load application region. The transfer of load or the load path from one H-section to the other should travel from the H-section to the joint through the cover plates and the bolts. Without providing a minimum clearance the load will be eccentrically loaded on the plates or the bolts in terms of early offset of irregular displacements. The testing is based on axial loading, so there should be a minimum clearance in each of the models being tested. The samples from model M-G25-H350 hold a clearance of 150mm on either side of the H-section. These samples are created based on the optimum utilization of the material available based on the length of the material that was procured by the distributor. The variation in length by a small portion of relative size, that is 50mm variation in length, may provide variation of compression testing parameters achieved by testing the samples from this model. The samples from model M-G25-H600 hold the length of each H-section as 600mm with a clearance of 400mm on either side. This model is well within the criteria of a short column, but

an increase in the height will induce slight buckling in the models. The effect of buckling in the compression testing parameters is derived by testing the samples from this model. The length of 600mm is selected based on the material acquired from the supply. These samples provide a clearance of 400mm from the point of load application. The difference or the dependence of parameters based on the length of the column is derived by testing the three models in this phase.

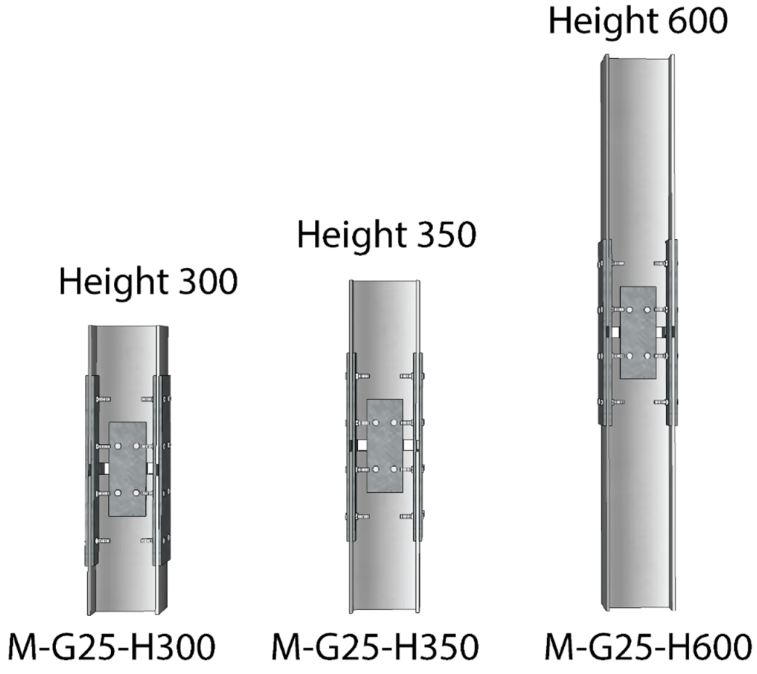

Fig. 2. Designs for model specimens of phase-2

3. Test Program

The models are created manually by cutting and drilling holes in H-sections and the cover plates based on the requirements of the design as shown in **Fig. 3**. The pitch and edge values for each connection will vary based on the design specification that is selected for different models. The pitch value should be greater than at least two times the edge value is the criteria for splicing as provided in Eurocode 3. Based on these values the bolted connection is designed using M8 8,8 grade steel bolts by Eurocode 3 from BS EN 1990 and BS EN 1991 guidelines for splicing connection. The torque on the bolts is tightened to a value of 28Nm based on recommendations from BS EN 15048 for M8 8.8 grade steel bolts and bolted connections. The bolt holes are drilled in the plates and the H-section with an ample amount of clearance to accommodate the steel bolts. There are five samples created for every model. The fully assembled connections are loaded into the AMSLER compression testing machine that is connected to Avery 500kN load cell as shown in **Fig. 4.** Linear Variable Differential Transformers (LVDTs) are placed on both sides of the testing assembly and are connected to a computer to record the displacement values of the joints. The load variation is made with an increment of 0.2kN and the reading of loading and its corresponding displacement is recorded accordingly. This procedure is done for all the samples and the machines are calibrated and checked before conducting the test for each sample.

Fig. 3. GFRP H-sections cutting, drilling of holes, and manual model making

Fig. 4. Manual testing of the models using AMSLER compression testing machine

The Digital design of the models involved the design of the specification drawings and FEA modeling. The specification drawing is carried out in Auto CAD 2D and Auto CAD 3D. The material ideation of the design is developed in Sketch Up for experiencing accurate 3D graphics of each model. CATIA is used to generate the testable modeling of the design with parts segregation, dimensioning, and labeling of each part. CATIA is a strong design software that is convenient to design mechanical parts compared to designing such complex mechanical parts in any FEA software. ANSYS workbench is used to stimulate FEA results. The files from CATIA are imported into the ANSYS workbench by saving them in igs format.

The models are analyzed in Ansys Workbench as a static structure. Since the components of the models are labeled in CATIA the assignment of material property becomes easier and more accurate in ANSYS. Meshing is a vital part of FEA, and the required mesh value is generated using the trial-and-error method. For accurate boundaries of meshing, it is advised to try for 0.1 to 0.2 times the lowest dimension of the component for macro-objects. By testing various mesh sizes 8mm is selected as shown in **Fig. 5**, the required mesh size based on the accuracy of the results obtained and the processing speed of the computer in which ANSYS was running. The contact surface and boundary conditions are important aspects of running a valid FEA simulation. The contact surface between the cover plate and the GFRP section; between the bolt head and the cover plate; the screw and the cover plate are all considered hard surfaces. The load application is made in the negative X axis as the surface of the H-section on the opposite end is fixed. The load versus displacement graph is plotted by generating the results for every 10kN change in the load. The deformation diagram of models was shown in **Fig. 6**. The maximum load-bearing capacity and the displacement of that load are noted and tabulated accordingly.

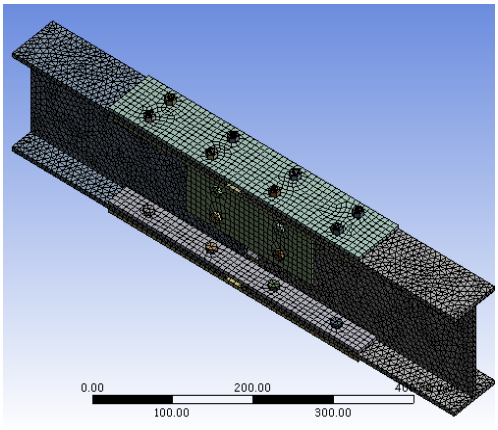

Fig. 5. Mesh analysis of 350 mm specimens

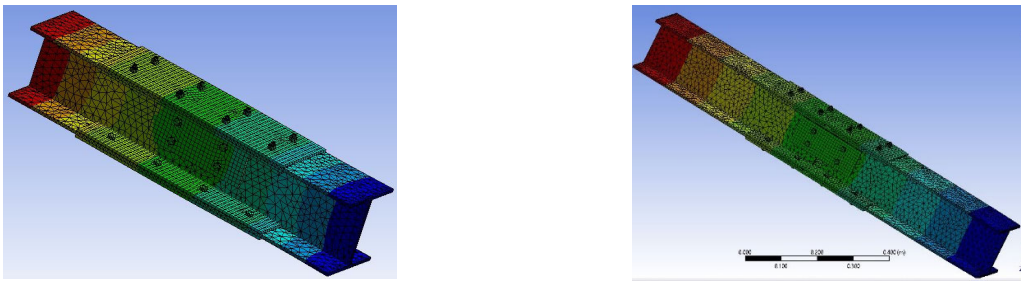

Fig. 6. FEA Deformation diagram for 300mm and 600mm specimens

4. Results and Discussion

An uncut GFRP H-section is crushed using FEA and Manual testing methods to analyze the strength of GFRP as a material. This value is compared with each of the connection designs to generate the percentage compressive strength of the connection. The Ultimate load of an uncut section when tested manually is determined to be 227.74 kN with a displacement of 0.78 mm and compressive strength of 122.18 N/mm2. The FEA ultimate load of the uncut section is determined to be 238.67 kN with a displacement of 0.81 mm and compressive strength of 128.04 N/mm^2. The stiffness of each model is calculated by considering the slope at 30% and 50% of the ultimate load from the load vs displacement graph that is plotted for each of the models. The load versus displacement graph for both manual testing and FEA un-cut section is provided in **Fig. 7.**

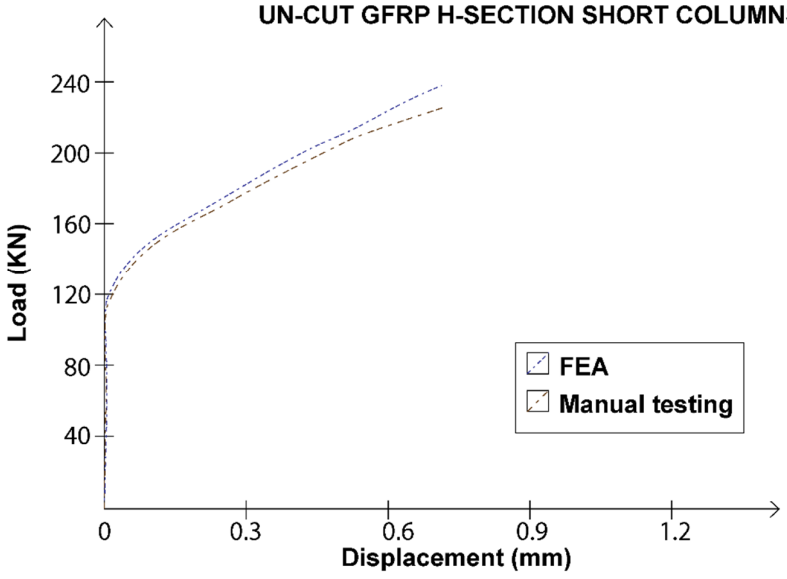

Fig. 7. Load versus displacement graph of the un-cut GFRP H-section

The Manual compression testing on each of the models is examined by the displacement and load values obtained from the computer-aided recordings based on the load cell values and LVDTs values. Each model is dissected to examine the modes of failure. The phase-1 results of the manual testing as represented in **Table 1** and the load versus displacement graph of each design is provided in **Fig. 8**. The models from M-G0-H350, which is a bearing spliced connection held an average ultimate load of 291.78 kN at an average displacement of 3.29 mm. The average stiffness of this connection is calculated to be 21.41 kN/mm with an average compressive strength of 151.99 kN/mm2. The FEA of M-G0-H350 failed at an ultimate load of 304.91 kN at a displacement of 2.48 mm and the stiffness of this connection is calculated to be 23.03 kN/mm with a compressive strength of 163.57 kN/mm^2. The models from M-G15-H350, which is a non-bearing spliced connection with a splicing gap of 15 mm, held an average ultimate load of 220.34 kN at an average displacement of 11.20 mm. The average stiffness of this connection is calculated to be 16.65 kN/mm with an average compressive strength of 118.19 kN/mm^2. The FEA of M-G15-H350 failed at an ultimate load of 230.34 kN at a displacement of 11.28 mm and the stiffness of this connection is calculated to be 17.76 kN/mm with a compressive strength of 124.10 kN/mm^2. The models from M-G25-H350, which is a non-bearing spliced connection with a splicing gap of 25 mm, held an average ultimate load of 211.44 kN at an average displacement of 11.66 mm. The average stiffness of this connection is calculated to be 15.86 kN/mm with an average compressive strength of 113.43 kN/mm^2. The FEA of M-G25-H350 failed at an ultimate load of 220.95 kN at a displacement of 12.15 mm and the stiffness of this connection is calculated to be 16.45 kN/mm with a compressive strength of 118.53 kN/mm^2. The models from M-G30-H350, which is a non-bearing spliced connection with a splicing gap of 30 mm, held an

average ultimate load of 205.09 kN at an average displacement of 12.41 mm. The average stiffness of this connection is calculated to be 15.35 kN/mm with an average compressive strength of 110.02 kN/mm2. The FEA of M-G30-H350 failed at an ultimate load of 213.65 kN at a displacement of 13.24 mm and the stiffness of this connection is calculated to be 15.79 kN/mm with a compressive strength of 114.61 kN/mm^2.

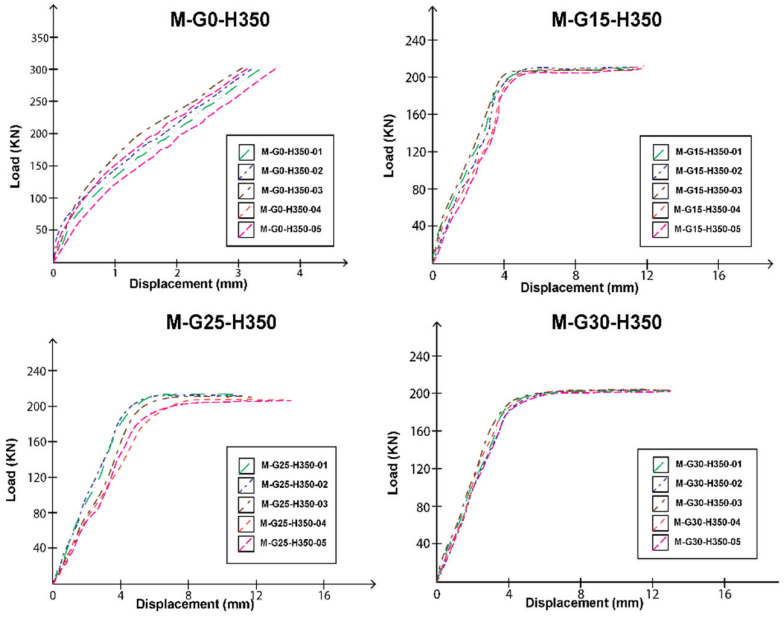

Fig. 8. Load versus displacement graphs of phase-1 samples

Table 1. Design characteristic properties of phase-1 models

Connection Design	Experimental Ultimate Displacement (mm)	Experimental Ultimate Load (kN)	Experimental Stiffness (kN/mm)	Experimental Compressive strength (kN/mm^2)	Failure modes
0mm Splicing Gap					
M-G0-H350-01	2.98	293.63	21.40	157.44	Bearing, Cleavage, Net Tension
M-G0-H350-02	3.41	289.10	21.49	155.01	Bearing, Cleavage
M-G0-H350-03	3.19	289.69	21.54	155.33	Bearing, Cleavage
M-G0-H350-04	3.31	295.10	21.35	158.23	Bearing, Cleavage, Net Tension
M-G0-H350-05	3.22	290.85	21.39	155.95	Bearing, Cleavage
15mm Splicing Gap					
M-G15-H350-01	11.89	219.06	16.92	117.46	Bering, Cleavage, Net Tension
M-G15-H350-02	11.95	220.43	16.39	118.19	Bering, Cleavage, Net Tension
M-G15-H350-03	11.79	221.98	.16.53	119.02	Bering, Cleavage, Net Tension
M-G15-H350-04	11.92	220.19	16.47	118.06	Bering, Cleavage, Net Tension
M-G15-H350-05	11.72	220.55	16.08	118.26	Bering, Cleavage, Net Tension
25mm Splicing Gap					
M-G25-H350-01	11.76	212.82	15.99	114.11	Bering, Cleavage, Net Tension
M-G25-H350-02	11.61	210.50	15.55	112.87	Bering, Cleavage, Net Tension
M-G25-H350-03	11.63	212.57	16.52	113.98	Bering, Cleavage, Net Tension
M-G25-H350-04	11.68	211.40	15.59	113.35	Bering, Cleavage, Net Tension
M-G25-H350-05	11.75	212.52	15.66	113.95	Bering, Cleavage, Net Tension
30mm Splicing Gap					
M-G30-H350-01	12.55	206.16	15.36	109.29	Bering, Cleavage, Net Tension
M-G30-H350-02	12.89	204.15	15.37	111.13	Bering, Cleavage, Net Tension
M-G30-H350-03	13.26	204.80	15.56	109.35	Bering, Cleavage, Net Tension
M-G30-H350-04	13.24	205.02	15.59	109.87	Bering, Cleavage, Net Tension
M-G30-H350-05	13.02	203.83	15.12	110.23	Bering, Cleavage, Net Tension

The phase-2 results of the manual testing as represented in **Table 2** and the load versus displacement graph of each design is provided in **Fig. 9.** The models from M-G25-H300, which is a non-bearing spliced connection with a splicing gap of 25

mm and an overall height of 625 mm with two H-sections each of 300 mm in height. These models held an average ultimate load of 220.32 kN at an average displacement of 10.94 mm. The average stiffness of this connection is calculated to be 16.65 kN/mm with an average compressive strength of 118.19 kN/mm^2. The FEA of M-G25-H300 failed at an ultimate load of 230.34 kN at a displacement of 11.30 mm and the stiffness of this connection is calculated to be 17.76 kN/mm with a compressive strength of 124.10 kN/mm^2. The models from M-G25-H350, which is a non-bearing spliced connection with a splicing gap of 25 mm and an overall height of 725 mm with two H-sections each of 350 mm in height. These models held an average ultimate load of 211.44 kN at an average displacement of 11.66 mm. The average stiffness of this connection is calculated to be 15.86 kN/mm with an average compressive strength of 113.43 kN/mm^2. The FEA of M-G25-H350 failed at an ultimate load of 220.95 kN at a displacement of 12.15 mm and the stiffness of this connection is calculated to be 16.45 kN/mm with a compressive strength of 118.53 kN/mm^2. The models from M-G25-H600, which is a non-bearing spliced connection with a splicing gap of 25 mm and an overall height of 1225 mm with two H-sections each of 600 mm in height. These models held an average ultimate load of 201.86 kN at an average displacement of 14.46 mm. The average stiffness of this connection is calculated to be 15.32 kN/mm with an average compressive strength of 107.75 kN/mm^2. The FEA of M-G25-H600 failed at an ultimate load of 212.77 kN at a displacement of 14.23 mm and the stiffness of this connection is calculated to be 15.89 kN/mm with a compressive strength of 114.14 kN/mm^2.

Table 2. Design characteristic properties of phase-2 models

Connection Design	Experimental Ultimate Displacement (mm)	Experimental Ultimate Load (kN)	Experimental Stiffness (kN/mm)	Experimental Compressive strength (kN/mm^2)	Failure modes
300mm H-section connection					
M-G25-H300-01	10.89	221.22	16.64	118.62	Bearing, Cleavage, Net Tension
M-G25-H300-02	11.01	220.24	16.73	118.09	Bearing, Cleavage, Net Tension
M-G25-H300-03	11.10	219.63	16.01	117.76	Bearing, Cleavage, Net Tension
M-G25-H300-04	10.61	221.01	16.24	118.50	Bearing, Cleavage, Net Tension
M-G25-H300-05	10.94	220.07	16.59	118.00	Bearing, Cleavage, Net Tension
350mm H-section connection					
M-G25-H350-01	11.76	212.82	15.99	114.11	Bering, Cleavage, Net Tension
M-G25-H350-02	11.61	210.50	15.55	112.87	Bering, Cleavage, Net Tension
M-G25-H350-03	11.63	212.57	16.52	113.98	Bering, Cleavage, Net Tension
M-G25-H350-04	11.68	211.40	15.59	113.35	Bering, Cleavage, Net Tension
M-G25-H350-05	11.75	212.52	15.66	113.95	Bering, Cleavage, Net Tension
600mm H-section connection					
M-G25-H600-01	14.10	201.15	14.96	108.18	Bering, Cleavage, Net Tension
M-G25-H600-02	14.34	202.51	15.31	107.74	Bering, Cleavage, Net Tension
M-G25-H600-03	14.18	203.31	15.70	108.32	Bering, Cleavage, Net Tension
M-G25-H600-04	14.50	202.20	15.24	109.16	Bering, Cleavage, Net Tension
M-G25-H600-05	14.39	201.41	15.42	108.73	Bering, Cleavage, Net Tension

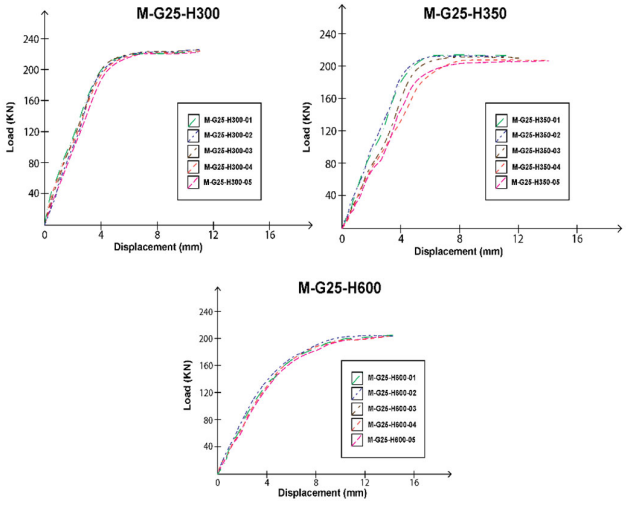

Fig. 9. Load versus displacement graphs of phase-2 samples

The Manual testing average values and FEA values for each model are provided in **Table 3**. Parameters such as Ultimate Displacement, Ultimate Load, Stiffness, and Compressive Strength are measured and calculated using both Manual Testing

and FEA. The results of both Phases are provided with a comparison of results between both testing methods. The comparison of manual testing and FEA load versus displacement graph of each phase models were shown in **Fig. 10** and **Fig. 11.**

Table 3. Manual testing and FEA results of the models

Connection Design	FEA ultimate displacement (mm)	Average Experimental ultimate displacement (mm)	FEA ultimate load (kN)	Average Experimental ultimate (kN)	FEA Stiffness (KN/mm)	Average Experimental stiffness (KN/mm)	FEA Compressive strength (kN/mm^2)	Average Experimental Compressive Strength (kN/mm^2)
Phase 1 Results								
M-G0-H350	2.48	3.22	304.91	291.67	23.03	21.43	163.57	156.39
M-G15-H350	11.85	11.20	230.34	220.44	17.76	16.48	124.10	118.20
M-G25-H350	12.15	11.68	220.95	211.96	16.45	15.86	118.53	113.65
M-G30-H350	13.24	12.99	213.65	204.79	15.79	15.40	114.61	109.97
Phase 2 Results								
M-G25-H300	11.30	10.91	230.34	220.43	17.76	16.44	124.10	118.19
M-G25-H350	12.15	11.66	220.95	211.44	16.45	15.86	118.53	113.43
M-G25-H600	14.23	14.30	212.77	202.12	15.89	15.33	114.14	108.43

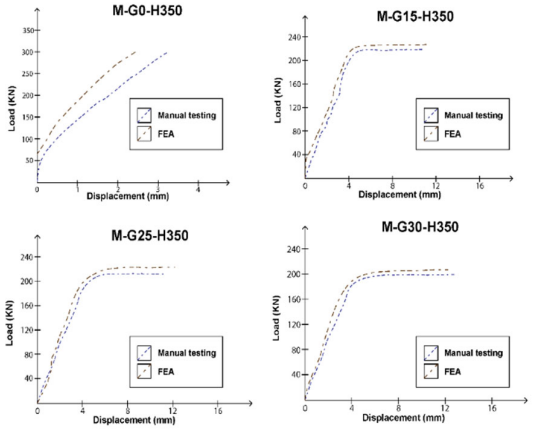

Fig. 10. Comparison of load versus displacement graphs of manual testing and FEA of phase-1 models

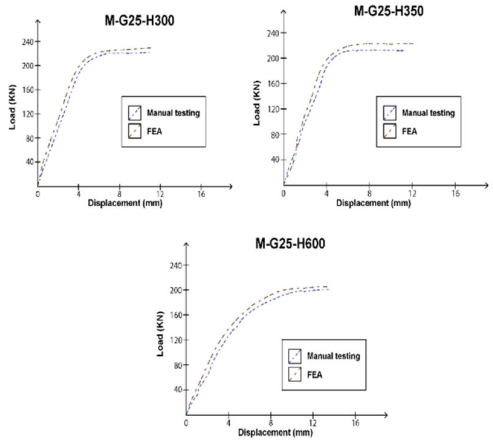

Fig. 11. Comparison of load versus displacement graphs of manual testing and FEA of phase-2 models

The percentage compression strength of each model compared to that of an un-cut GFRP H-section subjected to uniaxial compression loading is provided in **Table 4**. The bearing spliced connection of model M-G0-H350 is expressed to be the strongest when compared to other joint designs with a percentage compressive strength of 128.0% compared to that of an uncut GFRP H-section. Similarly, the FEA percentage compressive compared to an uncut GFRP H-section for these models is calculated to be 127.7%.

Table 4. Percentage compressive strength of models compared to that of an un-cut H-section

Connection design	Percentage Manual testing Compressive Strength compared To Un-cut H-Section(%)	Percentage FEA Compressive Strength compared To Un-cut H-Section (%)
	Phase-1	
M-G0-H350	128.0	127.7
M-G15-H350	96.7	96.5
M-G25-H350	93.0	92.5
M-G15-H350	89.9	89.5
	Phase-2	
M-G25-H300	96.7	96.5
M-G25-H350	92.8	92.5
M-G25-H600	88.7	89.1

5. Conclusions

Splicing is a form of connection that is provided in Eurocode 3 for connecting two or more steel sections. The principle of splicing is based on reinforcing the joint to provide additional strength to the region or area of connection. There are two forms of spicing which are Bearing and Non-bearing Splicing. Bearing spicing is a form of generic reinforcement of the connection joint which is achieved by using Cover plates and connection method. Non-bearing Splicing uses cover plates and connection methods with the concept of having a structural fuse in the joint. The fuse in the joint prevents the structure from

failing abruptly and imposes a concept of robustness making the structure more reliable and safer. GFRP as a material fails abruptly, so the connection designs established when designing structures using GFRP structures should be unique to tackle this aspect of the material.

In this study, the compressive strength and load tolerance of an un-cut GFRP H-section, bearing spliced connections, and non-bearing spliced connections are tested and compared to derive a reliable connection for GFRP short columns. Specimens are tested in two phases based on the length of the splicing can and the length of the short column. In Phase 1 four connection designs are established based on 0mm, 15mm, 25mm, and 30mm splicing gap. The connection design of a 0mm splicing connection is a bearing splicing connection. In this study, the models developed from this connection displayed the strongest design parameters with an ultimate load capacity of 291.67kN and 304.91kN when tested using manual testing and FEA accordingly. The percentage compressive strength of this connection design when compared to that of an un-cut GFRP H-section is 128% and 127.7% based on manual testing and FEA. The other three connection designs are developed using non-bearing splicing conditions. A minimum of 15mm is selected because the failure of these connections displayed an ultimate load displacement of 11.20mm to 14.30mm. The 25mm splicing gap is calculated by Eurocode 3 based on the column dimensions and the 30mm splicing gap is used to test the behavior beyond the Eurocode specification for the splicing gap. The compressive strengths of these three models are lower than that of bearing splicing connection with the strength ranging from 89.5% to 93.0% depending on the model and the type of testing. Although the non-bearing connection design displayed superior strength compared to that of the bearing connections, the failure behavior in the load versus displacement graph is linear with the absence of a yield point. GFRP as a material also displaces linear failure behavior which makes the material less reliable for construction usage. Therefore, using a connection that displaces similar linear failure cannot be considered a choice for having a robust structure. The connections from the 15mm splicing gap trigger early offset off additional reinforcement provided by the closure of the splicing gap. The 30mm splicing gap is inferior in all the test parameters compared to the other two non-bearing spliced connection designs. So, the 25mm splicing gap as calculated by Eurocode 3 from BS EN 1993-1-8 is selected as the appropriate connection design for testing short column criteria on the connections in Phase 2.

The Short column criteria in Phase 2 are calculated using the slenderness ratio criteria, which prompts that the ratio of effective length to the radius of gyration should be less than 10. The effective length parameter depends on the end conditions of the column and in this test case it is fixed on both sides. The radius of gyration is the square root of the ratio of the moment of inertia to the cross-sectional area. By calculating the effective length and the radius of gyration at the axis which is perpendicular to the plane of cross-section the height of the models in Phase 2 is determined. The three models tested in Phase 2 include heights of the column being 625mm, 725mm, and 1225mm respectively which includes the 25mm splicing gap. The shortest column with a height of 625mm displayed the highest load tolerance of 230.34kN compared to the other two connection designs which displayed load tolerance of 220.95kN and 212.77kN respectively. This implies the superiority of the connection requirement over the quantum of material available for load tolerance. The lower compressive strength values with the increase in height of the columns are caused by a factor of minute buckling induction in the columns. A small quantum of buckling is observed as a factor of the increase in height and due to the presence of the splicing gap in the joint. The manually tested materials displayed slight amounts of visually notable bending right before attaining ultimate load capacity. Therefore, the presence of a splicing gap induces long column parameters such as buckling in short columns with the increase in the height of the column causing a decrease in the effective behavioral parameters such as load capacity, compression strength, and stiffness.

The use of connection joints is an aspect of the trifecta which are reliability, robustness, and ease of attainment. These joints play a vital role in keeping the structure intact and providing a factor of safety when implemented in a habitual structure. The joint parameters tested in this study are focused on the GFRP H-sections being subjected to axial compression restrictions. The practical application of such joints should account for various loading conditions such as horizontal loading, eccentric loading, and dynamic loading. The connection parameters will vary when there are other structural components such as long columns, beams, and slabs in association with the short columns tested in this study. Using testing methods such as Manual testing and FEA all such conditions for using GFRP Spliced connection in building a stable structure should be further researched to establish the reliability of the material for construction usage.

Acknowledgment

REVA University supported the conduct of the tests, which is appreciated by the authors.

References

Al-Wandi, S., Ding, S., & Mo, J. (2017). An approach to evaluate delamination factor when drilling carbon fiber-reinforced plastics using different drill geometries: experiment and finite element study. *The International Journal of Advanced Manufacturing Technology*, *93*, 4043-4061.

Anand, R. S., & Patra, K. (2017). Mechanistic cutting force modelling for micro-drilling of CFRP composite laminates. *CIRP Journal of Manufacturing Science and Technology*, *16*, 55-63.

Ascione, F., Feo, L., & Maceri, F. (2010). On the pin-bearing failure load of GFRP bolted laminates: An experimental analysis on the influence of bolt diameter. *Composites Part B: Engineering*, *41*(6), 482-490.

Baha, S. (2015). Numerical investigation of the rivet installation in an adhesively bonded joint and the load transfer in a bolted/bonded hybrid joint. *SAE International Journal of Materials and Manufacturing*, *8*(1), 45-55.

Banea, M. D., Rosioara, M., Carbas, R. J. C., & Da Silva, L. F. M. (2018). Multi-material adhesive joints for automotive industry. *Composites Part B: Engineering*, *151*, 71-77.

Bodjona, K., Raju, K., Lim, G. H., & Lessard, L. (2015). Load sharing in single-lap bonded/bolted composite joints. Part I: Model development and validation. *Composite Structures*, *129*, 268-275.

Bodjona, K., Raju, K., Lim, G. H., & Lessard, L. (2015). Load sharing in single-lap bonded/bolted composite joints. Part I: Model development and validation. *Composite Structures*, *129*, 268-275.

Bois, C., Wargnier, H., Wahl, J. C., & Le Goff, E. (2013). An analytical model for the strength prediction of hybrid (bolted/bonded) composite joints. *Composite Structures*, *97*, 252-260.

Camanho, P. P., & Catalanotti, G. (2018). Mechanical Fastening of Composite and Composite–Metal Structures. *Joining of Polymer-Metal Hybrid Structures: Principles and Applications*, 187-202.

Carbas, R. J., Palmares, M. P., & da Silva, L. F. (2020). Experimental and FE study of hybrid laminates aluminium carbon-fibre joints with different lay-up configurations. *Manufacturing Review*, *7*, 2.

Cepero-Mejías, F., Curiel-Sosa, J. L., Blázquez, A., Yu, T. T., Kerrigan, K., & Phadnis, V. A. (2020). Review of recent developments and induced damage assessment in the modelling of the machining of long fibre reinforced polymer composites. *Composite Structures*, *240*, 112006.

Chen, Y., Yang, X., Li, M., Wei, K., & Li, S. (2019). Mechanical behavior and progressive failure analysis of riveted, bonded and hybrid joints with CFRP-aluminum dissimilar materials. *Thin-Walled Structures*, *139*, 271-280.

Chowdhury, N. M., Wang, J., Chiu, W. K., & Chang, P. (2016). Experimental and finite element studies of thin bonded and hybrid carbon fibre double lap joints used in aircraft structures. *Composites Part B: Engineering*, *85*, 233-242.

Curiel-Sosa, J. L., Tafazzolimoghaddam, B., & Zhang, C. (2018). Modelling fracture and delamination in composite laminates: Energy release rate and interface stress. *Composite Structures*, *189*, 641-647.

Esmaeili-Goldarag, F., Babaei, A., & Jafarzadeh, H. (2018). An experimental and numerical investigation of clamping force variation in simple bolted and hybrid (bolted-bonded) double lap joints due to applied longitudinal loads. *Engineering Failure Analysis*, *91*, 327-340.

Feito, N., Díaz-Álvarez, J., López-Puente, J., & Miguelez, M. H. (2018). Experimental and numerical analysis of step drill bit performance when drilling woven CFRPs. *Composite Structures*, *184*, 1147-1155.

Gamdani, F., Boukhili, R., & Vadean, A. (2019). Tensile behavior of hybrid multi-bolted/bonded joints in composite laminates. *International Journal of Adhesion and Adhesives*, *95*, 102426.

Geng, D., Liu, Y., Shao, Z., Lu, Z., Cai, J., Li, X., ... & Zhang, D. (2019). Delamination formation, evaluation and suppression during drilling of composite laminates: A review. *Composite Structures*, *216*, 168-186.

Girot, F., Dau, F., & Gutiérrez-Orrantia, M. E. (2017). New analytical model for delamination of CFRP during drilling. *Journal of Materials Processing Technology*, *240*, 332-343.

Goldarag, F. E., Barzegar, S., & Babaei, A. (2015). An experimental method for measuring the clamping force in double lap simple bolted and hybrid (bolted-bonded) joints. *Transactions of FAMENA*, *39*(3), 87-94.

Heidary, H., & Mehrpouya, M. A. (2019). Effect of backup plate in drilling of composite laminates, analytical and experimental approaches. *Thin-Walled Structures*, *136*, 323-332.

Heidary, H., Karimi, N. Z., & Minak, G. (2018). Investigation on delamination and flexural properties in drilling of carbon nanotube/polymer composites. *Composite Structures*, *201*, 112-120.

Hocheng, H., & Tsao, C. C. (2005). The path towards delamination-free drilling of composite materials. *Journal of materials processing technology*, *167*(2-3), 251-264.

Krishnaraj, V., Prabukarthi, A., Ramanathan, A., Elanghovan, N., Kumar, M. S., Zitoune, R., & Davim, J. P. (2012). Optimization of machining parameters at high speed drilling of carbon fiber reinforced plastic (CFRP) laminates. *Composites Part B: Engineering*, *43*(4), 1791-1799.

Kwon, D. J., Kim, J. H., Kim, Y. J., Kim, J. J., Park, S. M., Kwon, I. J., ... & Park, J. M. (2019). Comparison of interfacial adhesion of hybrid materials of aluminum/carbon fiber reinforced epoxy composites with different surface roughness. *Composites Part B: Engineering*, *170*, 11-18.

Li, H. S., Gu, R. J., & Zhao, X. (2017). Global sensitivity analysis of load distribution and displacement in multi-bolt composite joints. *Composites Part B: Engineering*, *116*, 200-210.

Liu, F., Lu, X., Zhao, L., Zhang, J., Hu, N., & Xu, J. (2018). An interpretation of the load distributions in highly torqued single-lap composite bolted joints with bolt-hole clearances. *Composites Part B: Engineering*, *138*, 194-205.

Liu, L., Zhang, J., Chen, K., & Wang, H. (2014). Combined and interactive effects of interference fit and preloads on composite joints. *Chinese Journal of Aeronautics*, *27*(3), 716-729.

Liu, S., Zhang, W., Wu, Y., & Chen, Y. (2013). The damage investigation of wedge-shaped electromagnetic riveting structure of cfrp/aluminium alloy. *Journal of Testing and Evaluation*, *41*(2), 188-193.

Lü, X., Zhao, J., Hu, L., & Wang, H. (2016). Effect of interference fits on the fatigue lives of bolted composite joints. *Journal of Shanghai Jiaotong University (Science)*, *21*, 648-654.

Makhdum, F., Phadnis, V. A., Roy, A., & Silberschmidt, V. V. (2014). Effect of ultrasonically-assisted drilling on carbon-fibre-reinforced plastics. *Journal of Sound and Vibration*, *333*(23), 5939-5952.

Marques, G. P., Campilho, R. D. S. G., Da Silva, F. J. G., & Moreira, R. D. F. (2016). Adhesive selection for hybrid spot-welded/bonded single-lap joints: Experimentation and numerical analysis. *Composites Part B: Engineering*, *84*, 248-257.

Paroissien, E., Lachaud, F., Schwartz, S., Da Veiga, A., & Barrière, P. (2017). Simplified stress analysis of hybrid (bolted/bonded) joints. *International Journal of Adhesion and Adhesives*, *77*, 183-197.

Phadnis, V. A., Makhdum, F., Roy, A., & Silberschmidt, V. V. (2013). Drilling in carbon/epoxy composites: Experimental investigations and finite element implementation. *Composites Part A: Applied Science and Manufacturing*, *47*, 41-51.

Rahmé, P., Landon, Y., Lachaud, F., Piquet, R., & Lagarrigue, P. (2011). Analytical models of composite material drilling. *International Journal of Advanced Manufacturing Technology*, *52*.

Raju, K. P., Bodjona, K., Lim, G. H., & Lessard, L. (2016). Improving load sharing in hybrid bonded/bolted composite joints using an interference-fit bolt. *Composite Structures*, *149*, 329-338.

Sadowski, T., Nowicki, M., & Golewski, P. (2019). The influence of the use of fasteners with different stiffness in hybrid joints subjected to complex mechanical loads. *Archives of Metallurgy and Materials*, 1263-1268.

Samaei, M., Zehsaz, M., & Chakherlou, T. N. (2016). Experimental and numerical study of fatigue crack growth of aluminum alloy 2024-T3 single lap simple bolted and hybrid (adhesive/bolted) joints. *Engineering Failure Analysis*, *59*, 253-268.

Selahi, E. (2019). Failure study of hybrid bonded-bolted composite single and double lap joints. *J. Stress Anal*, *3*(2), 37-46.

Shahkhosravi, N. A., Yousefi, J., Najfabadi, M. A., Minak, G., Hosseini-Toudeshky, H., & Sheibanian, F. (2019). Static strength and damage evaluation of high speed drilled composite material using acoustic emission and finite element techniques. *Engineering Fracture Mechanics*, *210*, 470-485.

Shetty, N., Shahabaz, S. M., Sharma, S. S., & Shetty, S. D. (2017). A review on finite element method for machining of composite materials. *Composite Structures*, *176*, 790-802.

Sorrentino, L., Turchetta, S., & Bellini, C. (2017). In process monitoring of cutting temperature during the drilling of FRP laminate. *Composite Structures*, *168*, 549-561.

Stone, R., & Krishnamurthy, K. (1996). A neural network thrust force controller to minimize delamination during drilling of graphite-epoxy laminates. *International Journal of Machine Tools and Manufacture*, *36*(9), 985-1003.

Suemasu, H., Naito, Y., Gozu, K., & Aoki, Y. (2012). Damage initiation and growth in composite laminates during open hole compression tests. *Advanced Composite Materials*, *21*(3), 209-220.

Turki, Y., Habak, M., Velasco, R., Aboura, Z., Khellil, K., & Vantomme, P. (2014). Experimental investigation of drilling damage and stitching effects on the mechanical behavior of carbon/epoxy composites. *International Journal of Machine Tools and Manufacture*, *87*, 61-72.

Voß, R., Henerichs, M., Rupp, S., Kuster, F., & Wegener, K. (2016). Evaluation of bore exit quality for fibre reinforced plastics including delamination and uncut fibres. *CIRP Journal of Manufacturing Science and Technology*, *12*, 56-66.

Wang, G. D., Melly, S. K., & Ahmed, S. K. (2018). Finite element study into the effects of fiber orientations and stacking sequence on drilling induced delamination in CFRP/Al stack. *Science and Engineering of Composite Materials*, *25*(3), 555-563.

Yoon, D., Kim, S., Kim, J., & Doh, Y. (2020). Study on bearing strength and failure mode of a carbon-epoxy composite laminate for designing bolted joint structures. *Composite Structures*, *239*, 112023.

Yuanxin, D., Yuan, L., Kaifu, Z., Ping, L., & Jian, L. (2015). Analysis of bolt-to-laminate interface friction in bolted composite joint with interference-fit. *Materials Research Innovations*, *19*(sup6), S6-42.

Zhang, H., Zhu, P., Liu, Z., Qi, S., & Zhu, Y. (2021). Research on prediction method of mechanical properties of open-hole laminated plain woven CFRP composites considering drilling-induced delamination damage. *Mechanics of Advanced Materials and Structures*, *28*(24), 2515-2530.

Zhang, K., Hu, J., Zou, P., Cheng, Y., Luo, B., & Cheng, H. (2019). Effect of secondary bending and bolt load on damage and strength of composite single-lap interference-fit bolted structures. *Journal of Composite Materials*, *53*(28-30), 4385-4398.

Zou, P., Li, Y., Zhang, K., Cheng, H., & Li, J. (2017). Influence of interference-fit percentage on stress and damage mechanism in hi-lock pin installation process of CFRP. *Journal of Composite Materials*, *51*(25), 3525-3538.

Zuo, Y., Cao, Z., Zheng, G., & Zhang, Q. (2020). Damage behavior investigation of CFRP/Ti bolted joint during interference fit bolt dynamic installation progress. *Engineering Failure Analysis*, *111*, 104454.